RSC Advances

PAPER

View Article Online
View Journal | View Issue



Cite this: *RSC Adv.*, 2023, **13**, 16671

# Unraveling the photophysical characteristics and biological applications of vinyl sulfones as viscosity sensors†

Onnicha Khaikate,[a] Thitima Pewklang,[a] Tunyawat Khrootkaew,[a] Kantapat Chansaenpak,[b] Prapassara Muangsopa,[a] Chutima Kuhakarn[c] and Anyanee Kamkaew*[a]

Received 10th April 2023
Accepted 15th May 2023

DOI: 10.1039/d3ra02354k

rsc.li/rsc-advances

For the first time, a series of vinyl sulfone-$NH_2$-based push–pull fluorophores (**4a–4d**) were introduced for their potential use in biological applications. The fluorophores **4a–4d** were readily synthesized upon reduction of the corresponding vinyl sulfones-$NO_2$ (**3a–3d**), which were prepared by sulfonylation of nitrostyrene. Both types of probes can be prepared in high yields through a few steps with minimal cost. In diverse solvents, probes **4a–4d** exhibited fluorescence with strong emission peaking around 403–490 nm. Additionally, the fluorescence intensity of probe **4d** rose approximately 85-fold with increasing viscosity. The probes **4a–4d** demonstrated good stability and photostability in a broad pH range. Moreover, probes **4a–4d** showed significantly improved biocompatibility compared to those derived from **3a–3d**. For cell imaging applications, the developed probes **4a–4d** exhibited much stronger blue fluorescence in cancer cells (HepG2) compared to **3a–3d**. In addition, probes **4a–4d** exhibited low cytotoxicity within 24 h toward both cancer and normal cells (HEK-293). Interestingly, probe **4d** showed great sensitivity to viscosity in cancer cells. As a result, readily prepared vinyl sulfone-$NH_2$-based push–pull fluorophores (**4a–4d**) offer a promising strategy for further development as cancer cell staining agents.



## Introduction

Vinyl sulfone scaffolds are useful synthetic targets[1] and display crucial roles in natural products and drug discovery.[2,3] They can be found in numerous lead compounds and drug candidates such as rigosertib (anticancer), recilisib (radioprotective), and k11777 (antiparasitic).[4] For the usefulness of vinyl sulfones, they also have intriguing chemical characteristics and serve as helpful intermediates for the production of structurally complex organic compounds.[5,6] As a consequence, a number of studies from many research groups were devoted to the development of novel and convenient synthetic approaches to access vinyl sulfone scaffolds.[7,8] Although the vinyl sulfone skeleton has been extensively explored from both the synthetic and biological points of view, to our knowledge, their photophysical and photochemical characteristics with regard to biological applications have not been thoroughly investigated.

Small molecule-based fluorescent probes are intriguing because of their explicit and simple synthesis, facile purification, and high fluorescence quantum yield.[9–11] Among the small π-conjugated molecular family, push–pull fluorophores are the best candidate for developing effective fluorescent chemosensors. Organic push–pull fluorophores are a category of π-conjugated molecules containing electron-donating (EDGs) and electron-withdrawing groups (EWGs). The push–pull system enables immediate interaction between the EDGs and EWGs *via* the π-system which can be called intramolecular charge transfer (ICT). In this regard, we and others developed small molecule-based fluorescent probes for biological applications such as cellular imaging and microorganism targeting.[12–14]

As a part of our continuing endeavour to develop fluorescent probes, we hypothesized that modification of the small molecule vinyl sulfones would affect its photophysical characteristics. Due to the lack of conclusive study on the photophysical and imaging features of vinyl sulfone, we present here the chemical reduction of non-fluorescent probes, vinyl sulfone-$NO_2$ (**3**), to fluorescent probes, vinyl sulfone-$NH_2$ (**4**). Following that, their photophysical characteristics and biological applications are investigated. Normally, variations in viscosity are detected during tumour development. Therefore, many viscosity probes were reported to monitor viscosity at the

[a]*School of Chemistry, Institute of Science, Suranaree University of Technology, Nakhon Ratchasima 30000, Thailand. E-mail: anyanee@sut.ac.th*

[b]*National Nanotechnology Center, National Science and Technology Development Agency, Thailand Science Park, Pathum Thani 12120, Thailand*

[c]*Department of Chemistry and Center of Excellence for Innovation in Chemistry (PERCH-CIC), Faculty of Science, Mahidol University, Rama 6 Road, Bangkok 10400, Thailand*

† Electronic supplementary information (ESI) available: Materials and methods, syntheses and characterisations of all compounds, solvatochromism study, DFT calculations, cytotoxicity assays, and confocal experiments. See DOI: https://doi.org/10.1039/d3ra02354k

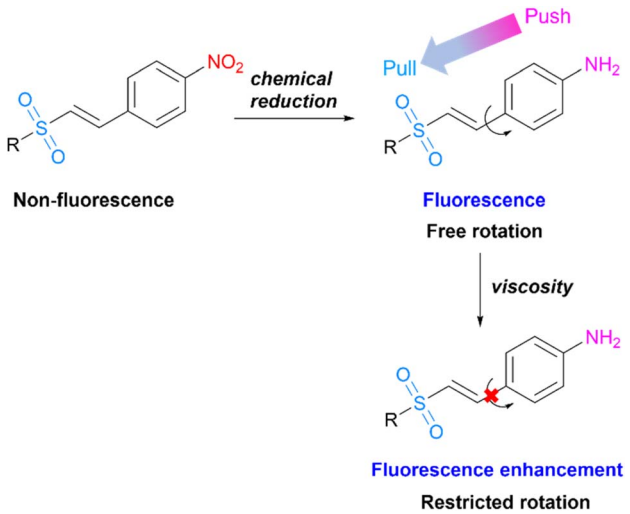


Scheme 1 Structural design of vinyl sulfone fluorescent probes and proposed mechanism for viscosity response.

cellular level.[15–18] From this point, fluorescent probes **4** are being explored for their capacity to detect changes in the microenvironment of cancer cells. We anticipate that in low-viscous fluids, the C–C bond of probe **4** will rotate freely, resulting in a non-radiative process of the excited state that would quench the fluorescence. Since rotation is restricted in a high-viscous environment, the fluorescence of the probe is projected to increase[15] (Scheme 1).

## Results and discussion

### Synthetic procedures

Vinyl sulfone-$NO_2$ probes (**3a–3d**) were designed to allow their synthesis from various sulfonyl hydrazides (**1**) and 4-nitrostyrene (**2**). Substrates **1** with electronically different substituents on the phenyl ring, including *p*-methyl, *p*-bromo, and naphthalene-2-sulfonyl hydrazide (**1d**) were selected for evaluation of their effects on the photophysical properties. Moreover, styrene-bearing nitro moiety at the *para* position was chosen as a coupling part because it will be employed as a molecular design for the reduction in the next step. The vinyl sulfones-$NO_2$ (**3a–3d**) were synthesised *via* sulfonylation of 4-nitrostyrene (**2**) (Scheme 2), according to a previously reported methodology.[19] The reaction between substrates **1** and **2** provided the corresponding products **3a–3d** in moderate to excellent yields. All products were characterized by $^1$H-NMR and $^{13}$C-NMR (see the ESI† for details).

### Photophysical properties of vinyl sulfones-$NO_2$ (3a–3d)

The photophysical properties of vinyl sulfones-$NO_2$ (**3a–3d**) were measured in different solvents including toluene, chloroform, tetrahydrofuran (THF), dichloromethane (DCM), dimethyl sulfoxide (DMSO), *N*,*N*-dimethylformamide (DMF), acetone, acetonitrile (MeCN), methanol (MeOH), DI water and 10 mM PBS buffer (pH 7.4). Compounds **3a–3d** exhibited the maximum absorbance at a wavelength ranging from 258 to 332 nm in all tested solvents (Table S1 and Fig. S2†). However, as shown in Fig. S3,† only the weak fluorescence emission of the four probes was observed. Nitroaromatic compounds are typically non-fluorescence as their photo mechanism involves fast or ultra-fast non-radiative deactivation of the electronically excited singlet states, increasing intersystem crossing to triplet excited states.[20] Therefore, we envisioned that the electronic properties of **3a–3d** would alter after the nitro group was reduced, resulting in a push–pull effect in the structures that would produce light.

### Chemical reduction of nitro groups to amines

To improve the photophysical properties *via* electron push–pull effects of vinyl sulfones-$NO_2$ (**3a–3d**), the nitro group was chemically reduced to amines *via in situ* hydrogen gas generation catalysed by $SnCl_2$ under sonication or microwave (Scheme 3). This reaction produced the corresponding vinyl sulfones-$NH_2$ (**4a–4d**) in moderate to excellent yields. All products were analysed by $^1$H-NMR, $^{13}$C-NMR, and HRMS (see the ESI† for details). In our probe design, **4a–4d** have electron push–pull effects between the amino and sulfone groups. In this work, only amino moiety located at the *para* position on substrates

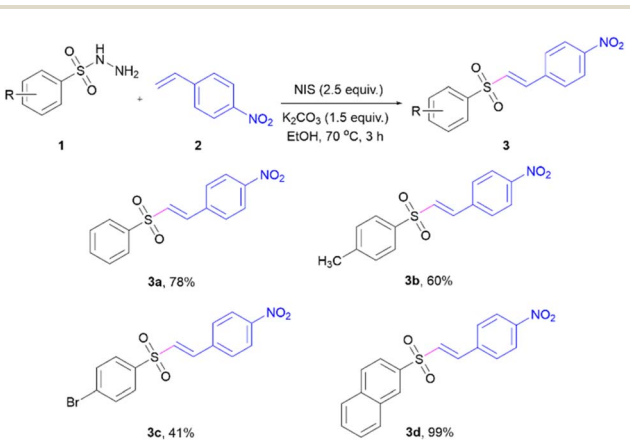


Scheme 2 Synthesis of vinyl sulfones.

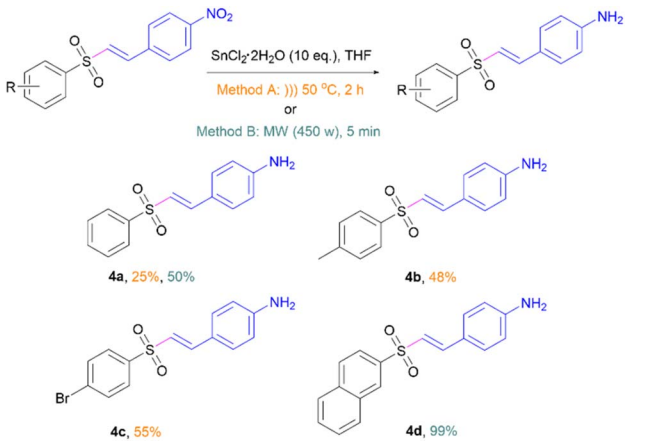


Scheme 3 Chemical reduction of nitro groups to amines.

was investigated since it exhibited the highest donor ability through resonance effect compared to the other positions.[21]

### Photophysical properties of vinyl sulfones-$NH_2$ (4a–4d)

Push–pull chromophores are widely recognized for significantly changing their absorption and emission patterns in solvents with various polarities. Since **4a–4d** contain both electron-donating and electron-accepting groups, they possess a typical D–π–A structure. Therefore, we studied their spectral properties in various solutions, and the results are summarized in Table S2.† As shown in Fig. S4,† the absorption spectra of **4a–4d** displayed negligible changes in different solvents. In contrast, probes **4a–4d** demonstrated fluorescence enhancement peaking around 403–490 nm in different solvents (Fig. S5†). As the solvent polarity increased from toluene to PBS buffer (pH 7.4), the fluorescence emission peaks of both **4a** and **4b** gradually red-shifted from 403 nm to 452 nm due to the dipole–dipole interaction between solute and solvent,[22] showing a stunning bathochromic effect (Fig. 1A and B).

In the meantime, observation of a broadening of the emission bands in polar solvents and an evident reduction in the fluorescence quantum yield ($\Phi_f$) indicate a twisted intramolecular charge-transfer (TICT) character for the excited state.[23] Obviously, probes **4d** exhibited abnormally blue-shifted fluorescence emission peaks in DI water and PBS relative to other high polar solvents (DMSO, DMF, acetone, MeCN, and MeOH) due to molecular aggregation (Fig. 1D).[24] In addition, probe **4c** in polar solvents, DMSO, DI water, and PBS, showed emission peaks around 455 nm along with shoulder peaks around 504 nm (Fig. 1C). Similarly, probe **4d** in DMSO, DMF, acetone, MeCN, MeOH, DI water, and PBS exhibited fluorescence spectra with two emissive peaks. Dual emission might originate from locally excited (LE) and intramolecular charge transfer (ICT) states, which is common for push–pull fluorophores. Their theory was based on the dynamics of excited states, which included local competition between excited states, intersystem crossover to the triplet state, emission from the ICT state, and ultimately deactivation *via* the non-emissive excited charge-separated state.[25,26] Another explanation for the observed behaviors might be related to the derivatives' ability to generate excimers, which is clear in the case of the naphthalene derivative. The molecular excimers are excited dimers that are created when there is a close proximity between two molecules that are interacting, one of which is in an excited state and the other of which is in the ground state. This results in a redistribution of the intensity of the monomer/excimer emission.[27,28] It is noteworthy that vinyl sulfones-$NH_2$ **4a–4d** in all solvents display Stokes shifts between 68 and 127 nm and fluorescence emission wavelengths between 403 and 490 nm. Regarding fluorescent quantum yield ($\Phi_f$), their emissions exhibit a considerable solvent dependence.

Next, the relationship between the Stokes shift ($\Delta\nu$) and the solvent orientation polarizability ($\Delta f$) was investigated using the Lippert–Mataga equation to evaluate the solvatochromism of the **4a–4d**.[29] The $\Delta\nu$–$\Delta f$ plots in Fig. S6† reveal that the slopes of the fitting lines for **4a–4d** are as large as 5208.2, 4158.4, 5910.8, and 9409.3 respectively. The large slope of the fitting line for **4d** suggests that **4d** possesses strong solvatochromism.[30] This offers strong support for the **4d**'s ability to serve as appropriate solvent polarity indicators.

### Fluorescence response to solvent viscosity

Because fluorescence quenching can occur from rotatable single bonds and excited-state C=C double bonds of **4** in a low-viscosity solvent, this phenomenon results in a nonplanar structure and energy loss *via* nonradiative pathways. However, because of the restrictions imposed by high-viscosity solvents, excited-state C=C double bonds, and rotatable single bonds in **4** were rigid, resulting in restricted intramolecular rotation (RIR) that increased fluorescence.[31] To test the hypothesis, we measured the emission spectra of vinyl sulfones-$NH_2$ (**4a–4d**) in a system containing water and glycerol. The viscosities of the solutions were raised from pure DI water to pure glycerol by increasing the amount of glycerol in the DI water. From the results shown in Fig. 2A–D, it can be found that **4a–4d** exhibited negligible fluorescence in pure DI water. While the emission intensity around 435 nm gradually increases with the increase of solution viscosity. Prominently, the fluorescence intensity

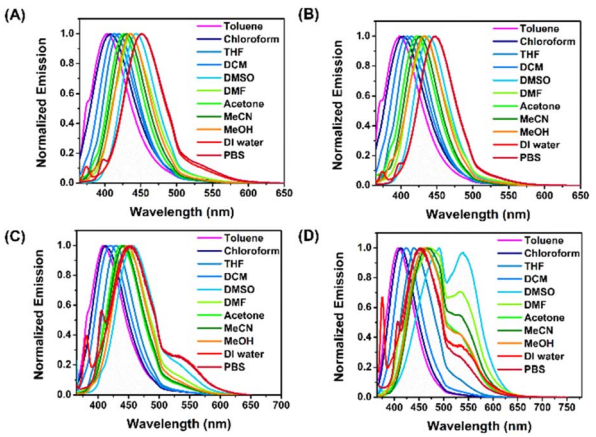


Fig. 1 Fluorescent spectra (excited at $\lambda_{max}$ of each solvent) of (A) **4a**, (B) **4b**, (C) **4c**, and (D) **4d** (10 μM) in different solvents.

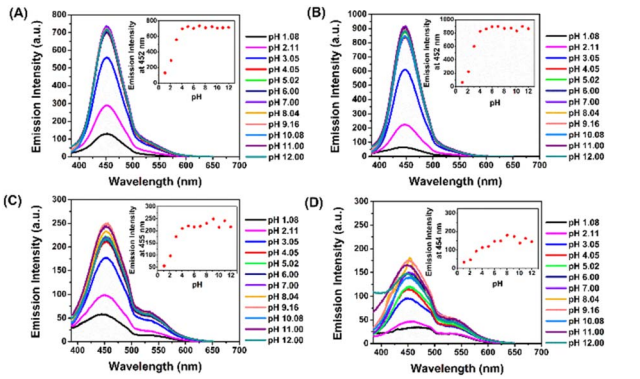


Fig. 2 Fluorescence spectra of (A) **4a**, (B) **4b**, (C) **4c**, and (D) **4d** (10 μM) in pH 1–12 buffers.

was enhanced by *ca.* 85-fold upon excitation at 315 nm, and the quantum yield changed from 0.0005 to 0.015, which belongs to probe **4d**.

### pH effects of vinyl sulfones-$NH_2$ (4a–4d) by fluorescence spectroscopic analysis

The probes **4a–4d** were also examined changes in the optical properties under different pH, owing to its pH-responsive functional group, the amino group. This pH-responsive moiety may undergo protonation, which can lead to changes in its electronic properties and consequent variations in emission intensity. To demonstrate this, the emission responses of **4a–4d** were evaluated. As shown in fluorescent spectra (Fig. 3A–D), all four probes exhibited a gradually significant decrease in fluorescence intensity with pH below 3. This phenomenon could be caused by the reduction of electron-donating characteristics, leading to a breakdown of the electron push–pull effect. On the other hand, emission intensity was relatively steady over a wide range from 4 to 12, indicating that D–π–A structure was maintained. Based on these results, it can be concluded that probes **4a–4d** preserved their high fluorescence signals over a broad pH range, making them appropriate for cell imaging investigations.

### Photostability of vinyl sulfones-$NH_2$ (4a–4d)

Each probe was dissolved in DMSO and exposed for 30 minutes to a 100 W UV light (365 nm) at room temperature. The maximum absorbance of **4a**, **4b**, and **4d** was reduced by less than 10%, but **4c** absorbance was reduced by around 23% (Fig. 4A and C). In addition, there was some drop in fluorescence intensity. Compounds **4a** and **4b** exhibit comparable photostability, with around 22–23% photobleaching detected. Notably, **4c** exhibited the most photobleaching (44%), while **4d** is the series' most photostable compound (11% photobleaching) (Fig. 4B and D).

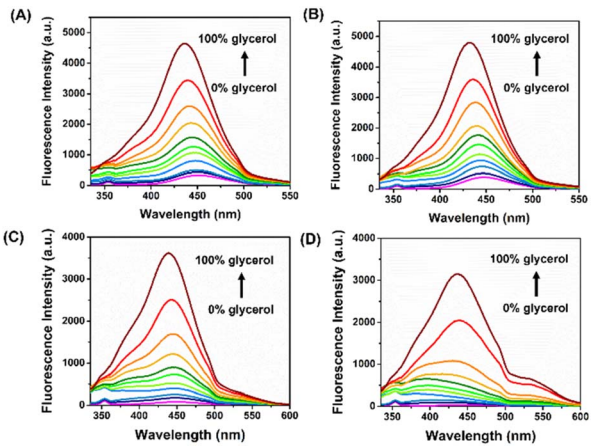


Fig. 3 Changes in the fluorescence emission spectra of (A) **4a**, (B) **4b**, (C) **4c**, and (D) **4d** (5 μM) with the variation of solution viscosity in the water/glycerol system ($\lambda_{ex}$ = 315 nm) and fluorescent intensity enhancement = 17-fold, 16-fold, 46-fold, and 85-fold for **4a**, **4b**, **4c**, and **4d**, respectively.

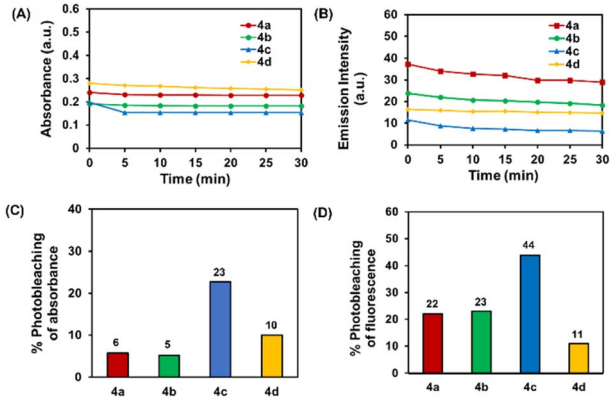


Fig. 4 Photobleaching studies at 250 W blue light monitored at the maximum (A) absorbance and (B) emission intensity of vinyl sulfones **4a–4d** in DMSO and calculated percentage of photobleaching based on (C) absorbance and (D) fluorescence intensity.

### Structural determination by DFT calculation

To gain a deeper understanding of the push–pull effect of vinyl sulfones-$NH_2$ (**4a–4d**), density functional theory (DFT) calculation was conducted using the Turbomole program. Geometric optimization was performed in the gas and water phases at the B3LYP/6-311G level and applied to calculate the frontier molecular orbital (FMO) energy. The FMO model is depicted in Fig. 5. In both the highest occupied molecular orbital (HOMO) and the lowest unoccupied molecular orbital (LUMO), the electronic charge distribution of **3a** mainly localized on the 4-nitrobenzene moiety, attributing to the weak electronic coupling between donor and acceptor. Unlike **3a**, LUMO orbitals of **4a–4d** were delocalized over 4-aminobenzene and sulfone moieties through the π conjugation while the HOMO orbitals were highly localized only on 4-aminobenzene due to the strong electron-donating character of $NH_2$. In addition, smaller HOMO–LUMO energy gaps (4.17 eV) in probe **4a** than in probe **3a** (4.41 eV) suggested a bathochromic shift in the emission wavelength. The other probes **4b–4d** also showed

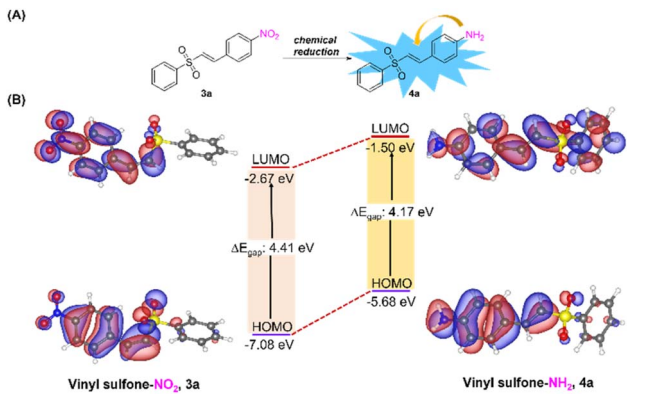


Fig. 5 (A) The proposed fluorescent mechanism of vinyl sulfone-$NH_2$ (**4a**) as compared to vinyl sulfone-$NO_2$ (**3a**). (B) HOMO–LUMO energy diagram in the gas phase of **3a** and **4a**, illustrating the intramolecular charge transfer (ICT) process.

similar profiles as depicted in Fig. S7 and S8.† To summarize, the theoretical calculation results were in good agreement with the experimental data, and the ICT process is crucial in changing the probe's optical properties.

### Cell viability

To be useful in biological applications, fluorescence probes must be non-toxic to cells. Thus, an MTT assay was used to assess cytotoxicity against cancer (HepG2) and normal (HEK-293) cells. When HepG2 cells were treated for 24 h with vinyl sulfones-$NO_2$ (**3a–3d**), the cells maintained more than 85% viability at concentrations up to 5 μM, as shown in Fig. 6A. At the highest concentration (40 μM), cell viability dropped to less than 20%, except for **3d**, about 70% viability was still observed at 40 μM. The results showed that **3a–3d** were quite toxic to the cells. On the other hand, when the nitro derivatives were reduced to vinyl sulfones-$NH_2$ **4a–4d**, no significant cytotoxicity was observed at doses up to 40 μM (>80% cells survival, Fig. 6B). For the normal cells, the cytotoxicity patterns were similar. When HEK-293 cells were treated with various concentrations of **3a–3d**, the cell viability significantly decreased to about 50% at the concentration of 40 μM (Fig. S9A†). Whereas more than 75% of HEK-293 cells survived upon incubation with **4a–4d** (up to 40 μM) for 24 h (Fig. S9B†), indicating that vinyl sulfones-$NH_2$ probes are suitable for cell imaging applications.

### Confocal imaging

To demonstrate the capability of vinyl sulfones-$NO_2$ (**3a–3d**) and vinyl sulfones-$NH_2$ (**4a–4d**) to be cancer cell staining probes, a laser confocal microscope was used for monitoring the fluorescence images. Time-dependent intracellular internalization was firstly examined by incubation of HepG2 cells with **3a–3d** and **4a–4d** (20 μM) for 0–6 h, followed by imaging. The findings shown in Fig. S10† reveal that even after 6 hours of incubation, there was no fluorescence signal in the HepG2 cells treated with vinyl sulfones-$NO_2$ (**3a–3d**). In contrast, after 1 h of incubation, vinyl sulfones-$NH_2$ (**4a–4d**) displayed bright fluorescence in the blue channel, particularly probes **4c** and **4d**, which had much greater blue fluorescence as seen in Fig. 7A and C.

Next, dose-dependent intracellular internalization was also studied for comparison. The cells were treated with 0–20 μM of

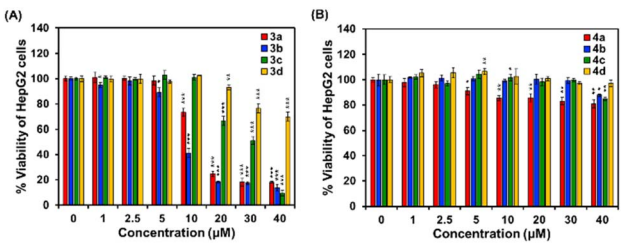


Fig. 6 Cytotoxicity assays of (A) vinyl sulfones-$NO_2$ (**3a–3d**) and (B) vinyl sulfones-$NH_2$ (**4a–4d**). HepG2 cells were treated at different concentrations for 24 h (error bar represents standard deviation, $n = 3$). Statistical analysis is based on $T$-test (*$P < 0.05$, **$P < 0.01$, ***$P < 0.001$), the control and each concentration were compared.

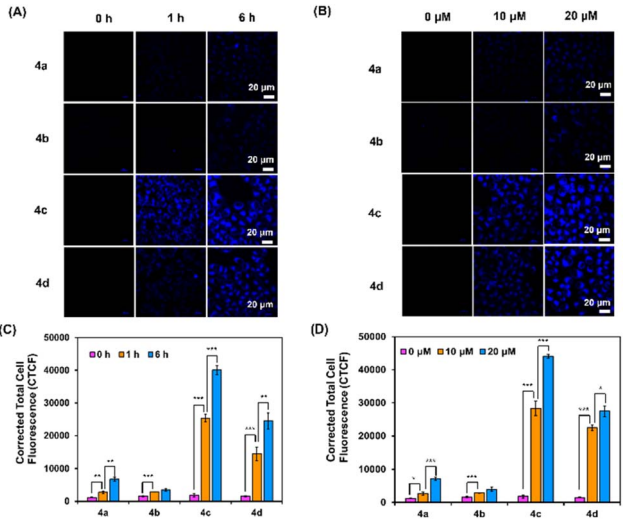


Fig. 7 (A) Confocal images of HepG2 cells incubated with vinyl sulfones-$NH_2$ (**4a–4d**) (20 μM) for 0–6 h. (B) Confocal images of HepG2 cells incubated with vinyl sulfones-$NH_2$ (**4a–4d**) (0–20 μM) for 6 h. Scale bar = 20 μm. (C and D) Corrected total cell fluorescence data of (A) and (B), respectively, qualified using ImageJ and represent the mean ± SD ($n = 30$). Statistical analysis is based on $T$-test (*$P < 0.05$, **$P < 0.01$, ***$P < 0.001$).

**3a–3d** and **4a–4d**, followed by a 6 hours incubation period. When the concentration was raised, compounds **4a–4d** showed strong fluorescence (Fig. 7B and D) while compounds **3a–3d** showed faint fluorescence at every concentration point (Fig. S11†). On the other hand, no fluorescence was observed from the control cells (HEK-293) after incubation with both **3a–3d** and **4a–4d** (Fig. S12†). These suggested that, in contrast to normal cells, cancer cells favoured the accumulation of the probes **3a–3d** and **4a–4d**. Therefore, vinyl sulfones-$NH_2$ (**4a–4d**) could be used to differentiate between cancerous and healthy cells.

As probes **4c** and **4d** offered bright fluorescence among the series, the intracellular localization of the probes was investigated. Colocalization experiments were examined with various fluorescent organelle trackers, including LysoTracker (for lysosome), MitoTracker (for mitochondria), ER-Tracker (for endoplasmic reticulum), and C6-NBD Ceramide (for Golgi apparatus), after 6 h exposure to **4c** and **4d**. As shown in Fig. 8, the blue emission signals from probes colocalized to some degree with LysoTracker, MitoTracker, and Golgi tracker (Pearson's $R$-value between 0.70–0.79). However, **4c** or **4d** overlapped more with the green signals from ER-Tracker, with a Pearson's correlation coefficient of 0.84 and 0.81, respectively, exhibiting favourable ER targeting in HepG2.

Since the spectroscopic analyses indicated that **4c** and **4d** exhibited environmental sensitivity behaviours, we further investigated their fluorescence response to changes in viscosity in cancer cells. To test whether probes **4c** and **4d** could identify changes in viscosity using fluorescence imaging, nystatin was used as an ionophore that could disrupt the ionic equilibrium and increase the viscosity.[32–34] Interestingly, compared to untreated cells, intracellular fluorescence enhanced about 2-

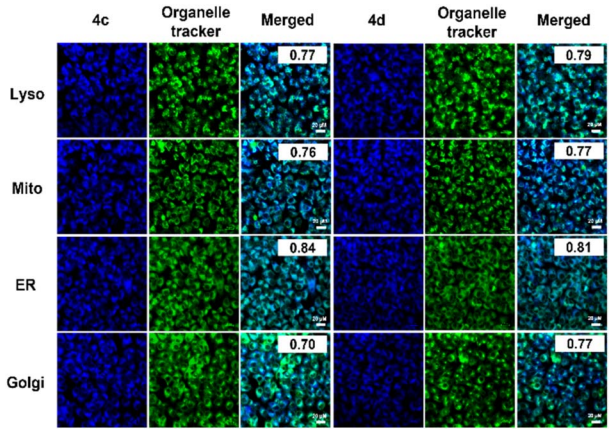


Fig. 8 Confocal images of HepG2 cells were incubated with **4c** and **4d** (20 μM) for 6 h and then incubated with organelle trackers: LysoTracker, MitoTracker, ER-Tracker, and NBD Ceramide (1 μM) for 10 min. Scale bar = 20 μm.

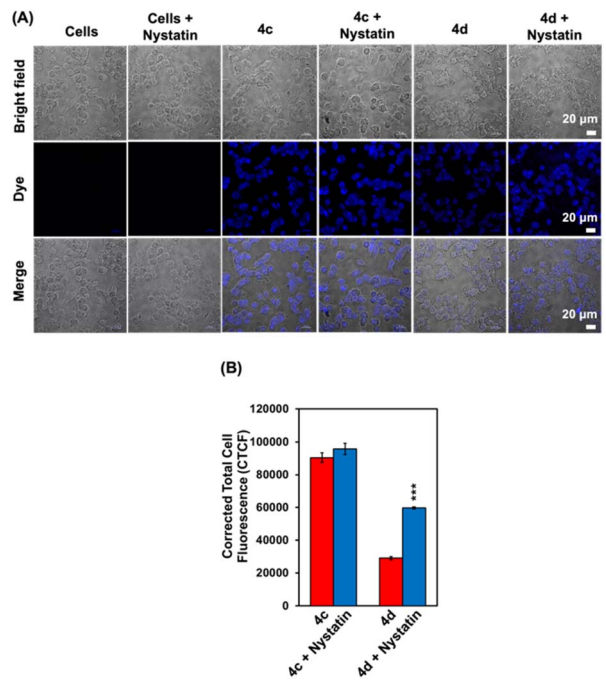


Fig. 9 (A) Confocal images of HepG2 cells incubated with **4c** and **4d** (20 μM) before and after incubation with nystatin (20 μM) for 30 min. (B) Corrected total cell fluorescence data qualified using ImageJ and represent the mean ± SD ($n$ = 30). Scale bar = 20 μm.

fold after the cells were pre-treated with nystatin followed by **4d** for 30 min (Fig. 9), while fewer changes were observed from **4c**. This result is consistent with the spectrometric analysis, which suggests the possible use of **4d** as a viscosity detection probe in cancer cells.

## Conclusions

In summary, we designed and synthesized the vinyl sulfones-$NH_2$ (**4a–4d**), containing electron-donating and electron-accepting groups, *via* a simple reduction from the corresponding vinyl sulfones-$NO_2$ (**3a–3d**) aiming to enhance the fluorescence emission through push–pull effects. The photophysical properties of these designed probes were systematically investigated, in which **4a–4d** exhibit fluorescence emission wavelengths between 403 and 490 nm and have Stokes shifts between 68 and 127 nm. Interestingly, among the series, the fluorescence intensity of **4d** showed an enhancement of about 85-fold with increased solvent viscosity. In addition, **4a–4d** illustrated stability in a wide range of pH, which are suitable for cell imaging applications. Moreover, probes **4a–4d** showed low cytotoxicity toward the HepG2 and HEK-293 cells, implying the biocompatibility of the probes. Cells were lightened by **4c** and **4d** from the first hour, according to time-dependent cellular uptake findings, and the fluorescence increased with extended time. Intriguingly, after 30 min incubation, intracellular fluorescence from **4d** increased about 2-fold after the viscosity of the cells increased, whereas **4c** showed very little change. Finally, co-localization experiments displayed that probes **4c** and **4d** were mainly located in the endoplasmic reticulum. With thorough spectroscopic investigations and computational calculations, we proposed that intramolecular charge transfer (ICT) plays a vital role in altering the **4a–4d** probes' optical characteristics, in which the intramolecular rotation in high-viscosity solutions is inhibited, resulting in fluorescence enhancement. As a result, this investigation offers a new powerful molecular design for the application of cellular environment change detection that is simply made in a few steps.

## Author contributions

O. K. synthesized and characterized all compounds. O. K., T. P., and P. M. conceived all the cell assays. T. K. performed DFT calculations. O. K., T. K., and A. K. prepared data visualizations. K. C., C. K., and A. K. validated the results. O. K. and A. K. wrote the first draft manuscript. All authors reviewed the manuscript.

## Conflicts of interest

There are no conflicts to declare.

## Acknowledgements

This work was supported by the Research and Development Fund, Suranaree University of Technology (SUT), Grant No. IRD1-102-65-12-22.

## Notes and references

1 G. Pandey, K. N. Tiwari and V. Puranik, *Org. Lett.*, 2008, **10**, 3611–3614.
2 F. Hof, A. Schütz, C. Fäh, S. Meyer, D. Bur, J. Liu, D. E. Goldberg and F. Diederich, *Angew. Chem., Int. Ed.*, 2006, **45**, 2138–2141.
3 S. Y. Woo, J. H. Kim, M. K. Moon, S.-H. Han, S. K. Yeon, J. W. Choi, B. K. Jang, H. J. Song, Y. G. Kang, J. W. Kim,

J. Lee, D. J. Kim, O. Hwang and K. D. Park, *J. Med. Chem.*, 2014, **57**, 1473–1487.
4 R. Ahmadi and S. Emami, *Eur. J. Med. Chem.*, 2022, **234**, 114255.
5 H. Kumamoto, K. Deguchi, T. Wagata, Y. Furuya, Y. Odanaka, Y. Kitade and H. Tanaka, *Tetrahedron*, 2009, **65**, 8007–8013.
6 S. Sulzer-Mossé, A. Alexakis, J. Mareda, G. Bollot, G. Bernardinelli and Y. Filinchuk, *Chem.–Eur. J.*, 2009, **15**, 3204–3220.
7 J. Meesin, P. Katrun, V. Reutrakul, M. Pohmakotr, D. Soorukram and C. Kuhakarn, *Tetrahedron*, 2016, **72**, 1440–1446.
8 Z. Zhan, H. Ma, D. Wei, J. Pu, Y. Zhang and G. Huang, *Tetrahedron Lett.*, 2018, **59**, 1446–1450.
9 S. Shanmugaraju and P. S. Mukherjee, *Chem. Commun.*, 2015, **51**, 16014–16032.
10 E. V. Verbitskiy, G. L. Rusinov, O. N. Chupakhin and V. N. Charushin, *Dyes Pigm.*, 2020, **180**, 108414.
11 R. F. Fatykhov, A. D. Sharapov, E. S. Starnovskaya, Y. K. Shtaitz, M. I. Savchuk, D. S. Kopchuk, I. L. Nikonov, G. V. Zyryanov, I. A. Khalymbadzha and O. N. Chupakhin, *Spectrochim. Acta, Part A*, 2022, **267**, 120499.
12 S. Wangngae, K. Chansaenpak, J. Nootem, U. Ngivprom, S. Aryamueang, R.-Y. Lai and A. Kamkaew, *Molecules*, 2021, **26**, 2979.
13 J. Chan, S. C. Dodani and C. J. Chang, *Nat. Chem.*, 2012, **4**, 973–984.
14 Y.-F. Wei, Y. Wang, X.-R. Wei, R. Sun, Y.-J. Xu and J.-F. Ge, *Spectrochim. Acta, Part A*, 2020, **229**, 117865.
15 P. Ning, P. Dong, Q. Geng, L. Bai, Y. Ding, X. Tian, R. Shao, L. Li and X. Meng, *J. Mater. Chem. B*, 2017, **5**, 2743–2749.
16 L. Chen, Y. Feng, Y. Dang, C. Zhong and D. Chen, *Anal. Bioanal. Chem.*, 2020, **412**, 7819–7826.
17 M. Ren, Q. Xu, S. Wang, L. Liu and F. Kong, *Chem. Commun.*, 2020, **56**, 13351–13354.
18 D. Su, C. Teoh, N. Gao, Q.-H. Xu and Y.-T. Chang, *Sensors*, 2016, **16**, 1397.
19 M. Pramanik, K. Choudhuri and P. Mal, *Asian J. Org. Chem.*, 2019, **8**, 144–150.
20 Y. M. Poronik, B. Sadowski, K. Szychta, F. H. Quina, V. I. Vullev and D. T. Gryko, *J. Mater. Chem. C*, 2022, **10**, 2870–2904.
21 S. Wangngae, T. Pewklang, K. Chansaenpak, P. Ganta, S. Worakaensai, K. Siwawannapong, S. Kluaiphanngam, N. Nantapong, R.-Y. Lai and A. Kamkaew, *New J. Chem.*, 2021, **45**, 11566–11573.
22 P. Xue, B. Yao, J. Sun, Q. Xu, P. Chen, Z. Zhang and R. Lu, *J. Mater. Chem. C*, 2014, **2**, 3942–3950.
23 J.-S. Yang, K.-L. Liau, C.-M. Wang and C.-Y. Hwang, *J. Am. Chem. Soc.*, 2004, **126**, 12325–12335.
24 P. Hiranmartsuwan, X. Ma, J. Nootem, R. Daengngern, A. Kamkaew, P. Pinyou, W. Wattanathana, V. Promarak, Z. Li and K. Chansaenpak, *Mater. Today Chem.*, 2022, **26**, 101121.
25 M. M. Khaled, M. A. Ismail, H. A. A. Medien, A. A. Abdel-Shafi and H. S. Abdel-Samad, *Spectrochim. Acta, Part A*, 2023, **288**, 122090.
26 E. Benassi, B. Carlotti, M. Segado, A. Cesaretti, A. Spalletti, F. Elisei and V. Barone, *J. Phys. Chem. B*, 2015, **119**, 6035–6040.
27 M. Pabst, B. Lunkenheimer and A. Köhn, *J. Phys. Chem. C*, 2011, **115**, 8335–8344.
28 A. S. Belova, Y. N. Kononevich, V. A. Sazhnikov, A. A. Safonov, D. S. Ionov, A. A. Anisimov, O. I. Shchegolikhina, M. V. Alfimov and A. M. Muzafarov, *Tetrahedron*, 2021, **93**, 132287.
29 N. Mataga, Y. Kaifu and M. Koizumi, *Bull. Chem. Soc. Jpn.*, 1956, **29**, 465–470.
30 J. Nootem, C. Sattayanon, S. Namuangruk, P. Rashatasakhon, W. Wattanathana, G. Tumcharern and K. Chansaenpak, *Dyes Pigm.*, 2020, **181**, 108554.
31 J. Liu, W. Zhang, C. Zhou, M. Li, X. Wang, W. Zhang, Z. Liu, L. Wu, T. D. James, P. Li and B. Tang, *J. Am. Chem. Soc.*, 2022, **144**, 13586–13599.
32 Z. Yang, Y. He, J.-H. Lee, N. Park, M. Suh, W.-S. Chae, J. Cao, X. Peng, H. Jung, C. Kang and J. S. Kim, *J. Am. Chem. Soc.*, 2013, **135**, 9181–9185.
33 O. HURŇÁK and J. Zachar, *Gen. Physiol. Biophys.*, 1995, **14**, 359–366.
34 M. J. Hansson, S. Morota, M. Teilum, G. Mattiasson, H. Uchino and E. Elmér, *J. Biol. Chem.*, 2010, **285**, 741–750.